Journal of Power Sources 195 (2010) 2691–2699

Contents lists available at ScienceDirect

Journal of Power Sources

journal homepage: www.elsevier.com/locate/jpowsour

Experimental investigation of water droplet–air flow interaction in a non-reacting PEM fuel cell channel

Angelo Esposito[a,b,*], Aaron D. Montello[a], Yann G. Guezennec[a], Cesare Pianese[b]

[a] Center for Automotive Research, The Ohio State University, Columbus, OH, USA
[b] Mechanical Engineering Department, University of Salerno, Fisciano (SA), Italy

ARTICLE INFO

Article history:
Received 22 May 2009
Received in revised form
25 September 2009
Accepted 18 November 2009
Available online 27 November 2009

Keywords:
Water droplet formation
Growth and detachment
Droplet–air flow interaction
Droplet oscillation
PEMFC
Frequency analysis

ABSTRACT

It has been well documented that water production in PEM fuel cells occurs in discrete locations, resulting in the formation and growth of discrete droplets on the gas diffusion layer (GDL) surface within the gas flow channels (GFCs). This research uses a simulated fuel cell GFC with three transparent walls in conjunction with a high speed fluorescence photometry system to capture videos of dynamically deforming droplets. Such videos clearly show that the droplets undergo oscillatory deformation patterns. Although many authors have previously investigated the air flow induced droplet detachment, none of them have studied these oscillatory modes. The novelty of this work is to process and analyze the recorded videos to gather information on the droplets induced oscillation. Plots are formulated to indicate the dominant horizontal and vertical deformation frequency components over the range of sizes of droplets from formation to detachment. The system is also used to characterize droplet detachment size at a variety of channel air velocities. A simplified model to explain the droplet oscillation mechanism is provided as well.

1. Introduction

While PEMFC technology has demonstrated significant advantages over other technologies, there remain many hurdles before widespread commercialization can take place. Some of the main matters requiring further advancement include: high cost of materials and manufacturing, expense and difficulty of fuel production, transport and storage, including a lack of widespread infrastructure. Moreover, water management within the PEMFC is still a critical aspect. It can be manifested in two forms, either as excess water, which leads to gas diffusion layer (GDL) and gas flow channel (GFC) flooding or as a shortage of water which leads to membrane dehydration. While each of these issues occur for alternate reasons, they can both result in significant reduction in FC stack power production as well as increasing the aging processes leading to stack degradation. From a technological standpoint, the issue of water management is therefore crucially important to increasing the commercial feasibility of PEMFCs and calls for further research.

There have been a great number of experimental studies performed on the water balance within the cathode GFC of the PEMFC. As detailed in their report on the many investigations of the topic published by Li et al. [1], the problem of flooding in PEMFC is not well understood, and there is also not a single widely applicable solution to the water management issue.

There are many types of physical measurements that can be employed to indicate the incidence of flooding. As water buildup in the cathode side flow channels of the fuel cell occurs, due to greater water production than efflux, gas flow passages become blocked. As the channels are increasingly restricted, an increase in the pressure drop across the channel also occurs. Several research efforts have employed techniques measuring the real-time pressure drop across the channel to identify the occurrence of flooding conditions [2,3].

Another possible indicator of problematic water flooding is the fuel cell output performance. As GFC flooding occurs, reactant gases are prevented from reaching the catalyst layer, thereby choking the electrochemical reaction and severely cutting output power. A method described in the literature uses a cell's product current to measure localized flooding with the use of a segmented current collector, which allows for the spatial resolution of current production [4]. However, difficulty arises as there are several problems that could occur within a fuel cell which would each result in significant losses of power. An example of such a problem is the exact opposite of the flooding problem, membrane dehydration. This causes a strong decrease in the membrane's electrical conductivity which causes significant output power reduction due to

* Corresponding author at: Mechanical Engineering Department, University of Salerno, via Ponte Don Melillo 1, 84084 Fisciano (SA), Italy. Tel.: +39 089 96 4239; fax: +39 089 96 4037.
E-mail addresses: angesposito@unisa.it, esposito.24@osu.edu (A. Esposito), pianese@unisa.it (C. Pianese).
URL: http://publicationslist.org/angesposito (A. Esposito).

0378-7753/$ – see front matter © 2009 Elsevier B.V. All rights reserved.
doi:10.1016/j.jpowsour.2009.11.078

Nomenclature

c	droplet chord (m)
CM	center of mass (m)
H	droplet height (m)
x	distance (m)
r	droplet radius (m)
f	frequency (Hz)
m	mass (kg)
S	surface area (m^2)
P	perimeter (m)
t	time (s)

Greek symbol

θ	contact angle (°)
μ	viscosity ($kg\,(m\,s)^{-1}$)
ρ	density ($kg\,m^{-3}$)
σ	surface tension ($N\,m^{-1}$)

Subscripts and superscripts

ad	advancing
rc	receding

drastic increases in ohmic losses. Some research efforts have made use of this increase in electrical resistance by measuring both the localized cell output as well as the impedance response [5].

Pressure measurement, cell output performance measurement, and other related techniques can, with varying degrees of success, identify global or local water flooding situations. This knowledge can be used to alert the system to perform necessary operational strategies to alleviate the flooding condition. However, these techniques have significant limitations, they do not provide insight into the specifics of water transport within the channel. The methods discussed can be exploited for on-line PEMFC diagnostic strategies but they are not directly able to assess the dynamics of the problem. For this reason, these techniques are essentially unable to provide understanding of the water management issue, being merely able to monitor if flooding has occurred. While it is obviously not necessary to fully understand a problem to develop a useful solution, the work here has been conducted for the sake of gaining specific knowledge which may potentially lead to a better solution of this difficulty. To do this, it will be necessary to gain tools offering a greater ability to understand the air–water interaction which is central to the flooding issue at hand.

The focus of this research is to further understanding of the nature of the water migration process and to attempt to apply this knowledge for the sake of developing better water efflux techniques, and thereby increase fuel cell performance as well as the technological viability. Therefore, this work is an investigation of the dynamic behavior of liquid product water in the cross-flowing air stream along the GDL/GFC interface of PEMFCs. Its originality lies in processing the recorded videos with a frequency decomposition code to uncover the specific frequency components in each signal throughout the range of droplet sizes. These signals are used to determine the nature of droplet oscillation and to find a relationship between droplet size and frequency of oscillation.

It should be noted that the research work performed for this study comes as the next activity in the sequence of research efforts having taken place at The Ohio State University – Center for Automotive Research (OSU – CAR) and the University of Salerno (UNISA). Furthermore, this work is also performed to support the validation of ongoing modeling techniques [6].

2. Visualization techniques state of the art

A large number of studies have been conducted utilizing visualization techniques aimed at understanding the dynamics of the channel flooding problem. Visualization techniques can allow access to the elemental dynamics of the air–water interaction, an understanding of which is crucial to comprehend the fundamentals of the channel flooding problem. Several different imaging techniques, including some rather complex methods such as neutron imaging [7–10], nuclear magnetic resonance imaging [11,12] and X-ray imaging [13,14], have been applied to the study of this problem. For this work it was determined that a direct visualization technique would be employed. Direct methods are much more straightforward to employ, while simultaneously offering increased capability in certain areas over the other techniques mentioned. The main benefits of the direct photometric visualization study include high spatial resolution in 2-dimensions, as well as high temporal resolution, while requiring much less expensive, less complex and less dangerous equipment. It is important to remark that although in general in situ techniques are the most reliable and accurate ones, they are usually less quantitative than ex situ techniques for observing water droplets build-up in a PEMFC channel. On the other hand, ex situ techniques are mandatory to further in situ studies on active PEM fuel cells.

There have been a number of direct visualization water transport studies involving electrochemically active fuel cells. One of the earliest such studies was performed by Tüber et al. [15] and utilized a twin straight-channel PEMFC with a Plexiglas endplate to allow visualization of the GFCs from above. The authors described a setup in which the power output from the cell was used to quantify the FC performance, to determine at which point water buildup begins to have meaningful detrimental effect. Another example of an active fuel cell visualization study is that performed by Yang et al. [16]. In this work, a setup similar to that previously described was employed, this time with seven parallel straight channels rather than two. The researchers noted that product water migrates from the catalyst layer to the surface of the GDL and forms distinct droplets. A third example of a direct visualization study of an electrochemically active PEMFC is that performed by Ous and Arcoumanis [17]. As with the previous two examples, this experimental setup again had a Plexiglas base plate to allow for water transport visualization from above. However, unlike the previous examples this setup makes use of a single serpentine channel. A brief mention is made in the article about the phenomenon of droplet "wobble" which was observed.

Several experimental efforts have been performed which indicate that with some care, the environment and water transport behavior within an active cell can be mimicked with acceptable accuracy in a non-active setup. This can be very beneficial, as investigations involving non-active setups offer significant advantages over active cell arrangements. These benefits range from simplicity of design and operation to added visualization capability due to fewer constraints associated with the setup. Furthermore, non-active apparatus offer the possibility to control the operating parameters one at a time. The group of Bazylak et al. [18] discussed an experimental apparatus with a GFC positioned above the GDL that allowed for visualization of water behavior in the presence of the flowing air stream. This system used Fluorescein dye (0.1 mM) to enhance visualization which was again performed from above. On the other hand, Lister et al. [19] showed that dye concentrations near 0.05 mM do not affect the physical properties of the water. Another example of a non-active cell experimental apparatus is that employed by Kumbur et al. [20]. This apparatus is fairly comparable with that used by Bazylak et al. with a few changes increasing the controllability of the system. This system allowed for control of not only the incoming air velocity, but also its temperature and

relative humidity, as well as the temperature of the water reservoir and channel structure. The authors attempted to characterize the dependence of the contact angle hysteresis (Δ) on other droplet parameters such as height, chord length, and air flow velocity.

While there have been a number of visualization studies conducted, there have been very few published investigations involving water droplet growth on the GDL surface and the ensuing dynamic interaction with the cross-flowing air stream. The research effort most closely pursuing this question was presented by Theodorakakos et al. [21]. The authors also claimed that knowledge of the behavior and interaction of droplets in a flowing air stream has relevance to a number of scientific and engineering applications well beyond the scope of PEMFCs. The authors observed the quasi-steady deformation experienced by droplets subjected to these flow conditions and noticed that the droplet's shape undergoes oscillatory deformation preceding detachment.

The hereby illustrated literature review highlights the lack of specific or in-depth studies of the droplet oscillations induced by the air flow. Therefore, the objective of this work is to quantitatively evaluate the effects of the air flow on a droplet attached onto the GDL surface. Although, the presence of the channel walls may play an important role in the mechanisms behind such interaction, as a first approach, it was preferred to investigate the droplet oscillation and detachment induced by the air flow as an isolated process. Thus, a scaled-up channel was designed to ensure absence of walls effect. Therefore, this work may serve as a basis for further and more complex studies.

3. Nature of water production and transport in GFCs

As described in the previous section, water production at the catalyst layer of the fuel cell stack occurs at discrete sites. Over time, the continued localized water production results in growth of droplets at the GDL/GFC interface. Ideally, during normal operation water droplets are fed from beneath and continue to grow until they reach their critical size. This is the point when the drag force from the cross-flowing air stream surpasses the adhesion force holding them onto the GDL surface. Due to the imbalance of forces, the droplets detach from the surface and are blown away in the exhaust gas stream. The force of air drag on the water droplets is proportional to the cross sectional area of the droplet, as well as the air velocity squared. Thus, while the ideal case results in droplets growing to critical size and detaching, if the air velocity in the channel is below a certain level, the required critical size could be approximately equal to or greater than the channel cross section. Development of droplets of this size could then result in flooding problems within the channel. From this simple analysis, it would seem that a simple solution to the flooding issue could be to merely increase air flow velocity through the cathode channels. However, this introduces two new problems: (1) the potential for over-drying and dehydration of the system, and (2) a significant increase in the cost of operation of the stack. For these reasons, it is desirable to gain a greater understanding of the fundamentals of the problem to attempt a more effective and cheaper solution.

The profile of a water droplet seated on the GDL substrate in a static condition appears as seen in Fig. 1a. Droplets inside the FC channels are small enough that the effects of gravity are minimal compared with the strength of surface tension forces, thus the droplets retain a nearly spherical shape, as exhibited in the sketch. Some of the important geometric parameters of the droplet include its height (H) and chord length (c), as well as the static contact angle (θ), which is defined as the angle between the tangent line along the interface between liquid, solid and gas. If the contact angle is less than 90° the liquid is said to be wetting, if it is greater than 90° the liquid is said to be non-wetting. For the static case, the contact

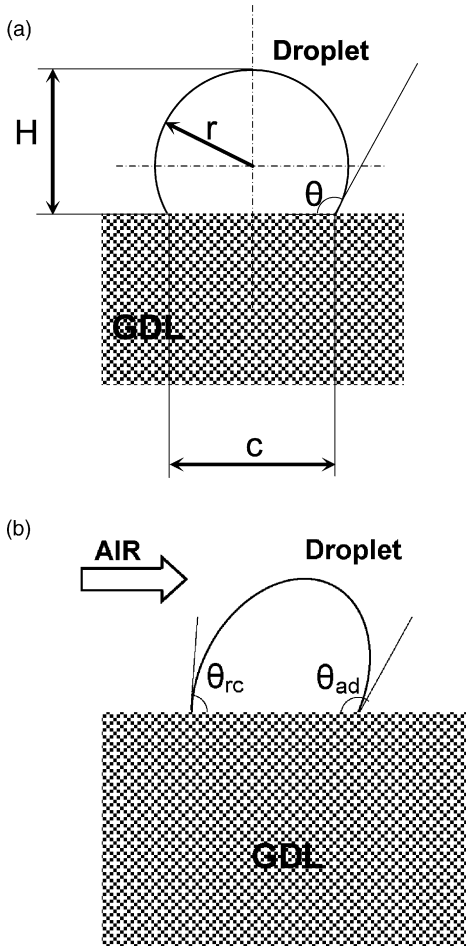

Fig. 1. Schematic of a water droplet seated on a GDL surface in (a) static and (b) dynamically deformed conditions.

angle is the same for both sides of the droplet and is a measure of the surface hydrophobicity.

In the case of the cross-flowing air stream, when the droplet is below the critical size, it deforms in the longitudinal direction approximately as seen in Fig. 1b. As can be seen, the left and right side contact angles deform and become the advancing (θ_{ad}) and receding (θ_{rc}) angles shown. The difference between these angles, known as contact angle hysteresis (Δ), is related to the surface adhesion force between the droplet and the surface. As a deformed droplet gets nearer its critical size, Δ will approach a threshold value, that when reached, will coordinate with droplet detachment. It is also worthwhile mentioning that the GDL is often treated with hydrophobic material (PTFE). Droplets on a hydrophobic surface have reduced chord length and hence cover fewer openings then the case of a hydrophilic surface. Furthermore, the water removal is enhanced. This is justified by the fact that the hydrophobic coating translates into contact angles greater than 90° and hence the water is non-wetting, which also means weaker adhesion force with respect to the wetting case. Thus, the water droplets on a hydrophobic surface are carried away more easily by the gas flow [22].

4. Experimental setup

To gain a greater understanding of the droplet growth and detachment process, an experimental apparatus was constructed to allow visualization of this phenomenon. For this setup, a schematic of which can be seen in Fig. 2, a physical model representative of

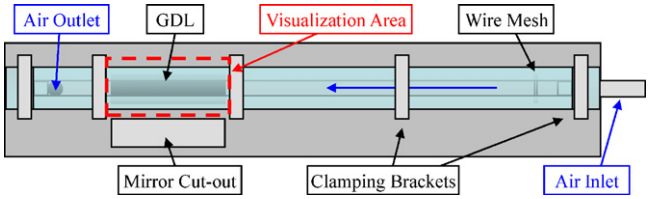

Fig. 2. Overhead schematic of experimental apparatus.

a fuel cell cathode channel was built. The setup features a single straight channel approximately 0.5 m long, allowing for the flow of air down the channel. The channel cross section was set at 13 mm wide by 13 mm tall, which represents a channel width scale up by about 10×. Water was delivered via capillary tubing connected to a syringe pump through a piece of carbon paper GDL material seated on the channel floor. The carbon papers tested included three configurations of Toray Paper 120, containing 5%, 10% and 20% PTFE. Of these three papers, there was noticeably different behavior of liquid water based on each paper's hydrophobicity. Since the interest of this work was to observe the case of individual droplets on the surface, the 20% PTFE paper was chosen as droplets on its surface exhibited greater tendency to detach in the air stream, rather than coalescing into films. The floor of the channel was machined from a block of aluminum, while the channel sidewalls and top were made from 13 mm thick Plexiglas. Visualization was enhanced through the use of Fluorescein dye dissolved in the water to a concentration of about 0.075 mM.

As the profile schematic in Fig. 3 shows, visualization was performed by illuminating the area of interest by three very bright 5-W blue LEDs, which allowed the marker to fluoresce very strongly. Side views of droplets were achieved through the use of a right-angle mirror in conjunction with a monochrome CCD camera with a 1.5× magnification lens. A yellow filter was placed in front of the lens to allow the droplets to appear much brighter than the rest of the image. A picture of the actual setup is illustrated in Fig. 4. For more details on the physical setup as well as specifics of components used, refer to chapter three of the M.S. Thesis by Montello [23].

5. Data processing

Through the setup described above, video sequences of droplets growing were recorded. Thanks to the high intensity of the illumination system, it was possible to capture videos at 500 frames per second (FPS) and greater. These videos clearly show that there is a significant amount of oscillation and "wobble" in sub-critical sized droplets. Such oscillatory motion has been noted briefly by Ous and Arcoumanis [17], as well as by Theodorakakos et al. [21], but it seems that no in-depth investigation of this motion appears anywhere in the literature.

The data processing carried out for this work is divided into two sections: image processing and data analysis. The first one involves extracting the desired information from the video, while the second portion involves analyzing the output of the image processing routine. Ultimately, both components together yield information about the dynamic behavior of water droplets as they form, grow, deform, oscillate and detach from the GDL surface in the experimental apparatus.

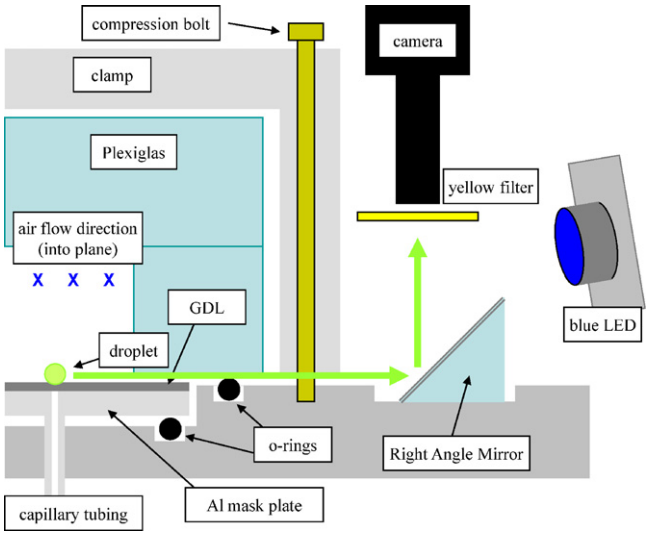

Fig. 3. Profile schematic of experimental channel apparatus.

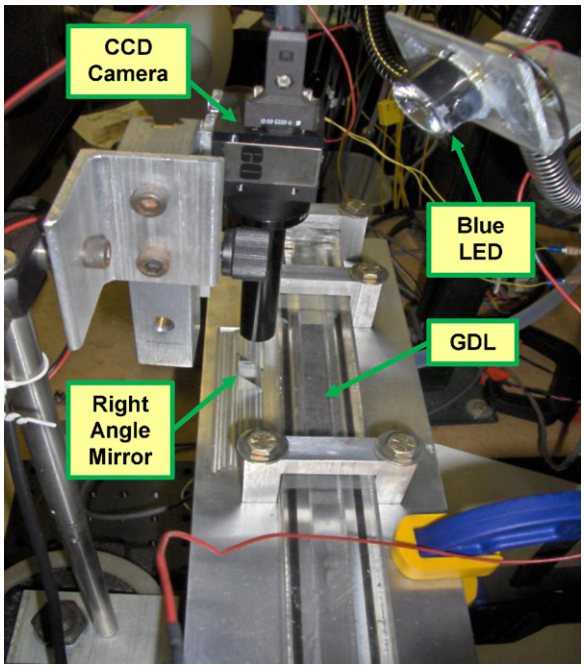

Fig. 4. Picture of the experimental setup.

5.1. Image processing

Using an ad-hoc image processing technique developed for this work, the 8 bit grayscale video sequences were converted to binary image sequences.

Fig. 5 shows a sequence of raw and processed frames to observe the dynamical deformation process which the droplet undergoes. In particular, the sequence contains 50 frames extracted from a section of a video captured with a frame rate of nearly 618 FPS. This sampling rate provides approximately 1.62 ms between frames, thus the entire sequence corresponds to about 81 ms of time. It should be noted that the droplet has detached in the second from last frame, as can be seen by the large displacement of the receding corner, and has begun to roll along the surface in the final frame. The frame sequence clearly illustrates the vibratory nature of droplet oscillation.

Once image were converted to binary, it was possible to perform a further processing to monitor the desired number of signals representative of the droplet size and shape.

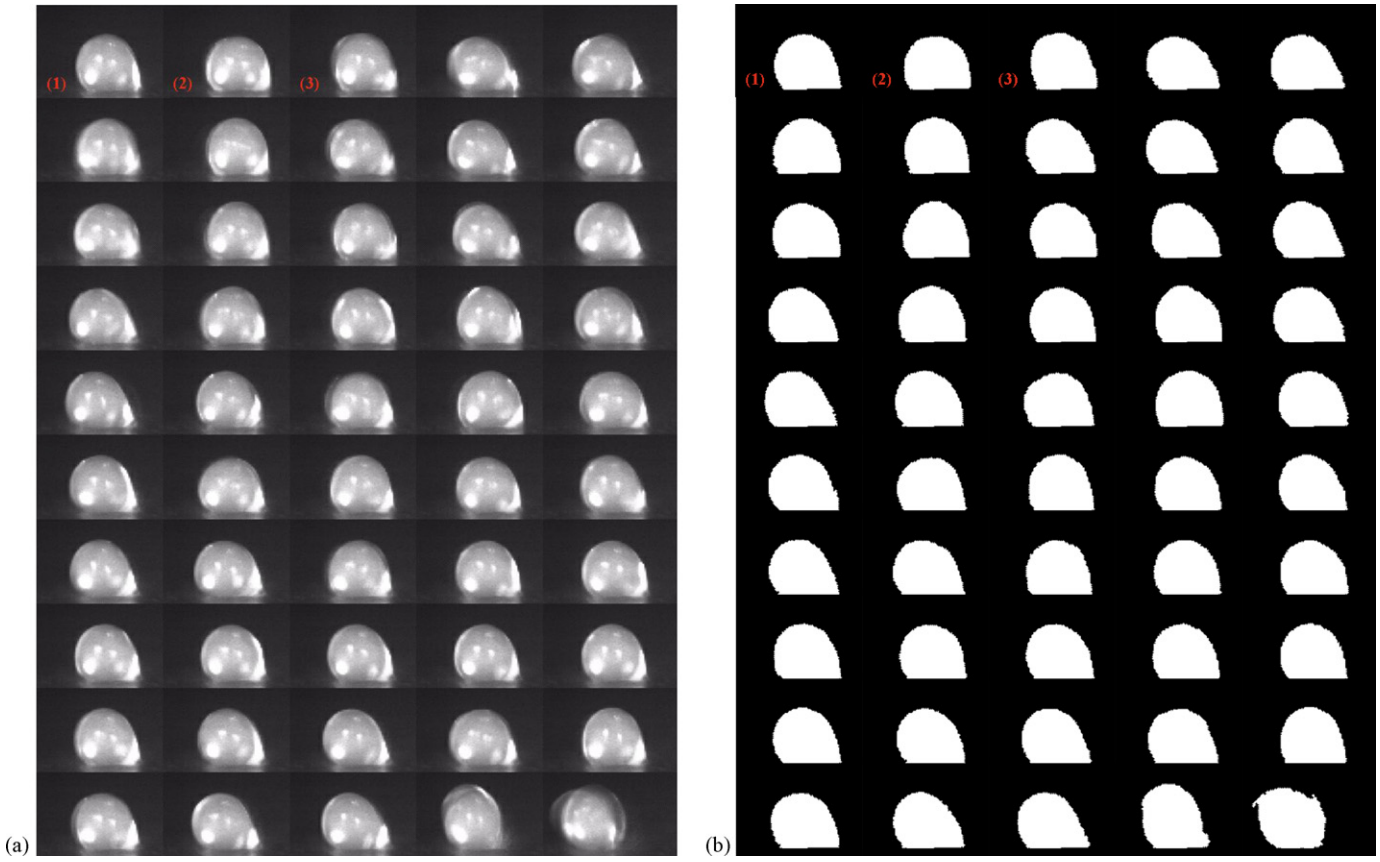

Fig. 5. Sequence of consecutive raw (a) and processed (b) frames with approximately 1.62 ms between frames.

5.2. Data analysis

The signals output from the image processing routine were exploited to characterize the time history of the evolution of the droplet size and shape and determine their significance.

The required data to be extracted from a single droplet image falls roughly into two categories: droplet properties which can be measured directly and those which can be calculated or estimated based on other parameters. In the first category are properties such as height, width and chord length, defined as the length of the contact line between the bottom of the droplet and the GDL surface. In the second category are the properties of droplet volume, air-contacting surface area, x and y centers of mass, contact angles, average contact angle, contact angle hysteresis for dynamically deforming droplets and contact patch, defined as the area of water contacting the GDL surface.

The plot in Fig. 6(a) shows an example of the droplet height recorded in time. It is worth highlighting that the droplet initial observable size is nearly 160 μm, well beyond the GDL mean pore size. As can be seen, the droplet clearly exhibits a vibratory motion as it grows over the approximately 800 ms lifetime. As expected, the size of the droplet has an impact on its oscillatory motion, so the signal was low-pass filtered and segmented by size with bins 0.0667 mm wide, overlapped of 50%, as represented by the green and yellow line pairs shown on the plot. Fig. 6(b) provides a magnification of the 0.500–0.566 mm height bin. The bins endpoints were recorded throughout the time sequence. These endpoints were then used to segment all other recorded signals. In this way, each of the signals representing droplet size and shape could be sectioned, with each segment corresponding to the behavior exhibited at a very narrow range in droplet size.

As an example, the segment endpoints for the 0.500–0.566 mm height bin are shown in Fig. 7 along with the section of the horizontal center of mass signal they represent. This section of data was then FFT filtered to determine the frequency components of oscillation existing there. The frequency spectrum can be seen in Fig. 8.

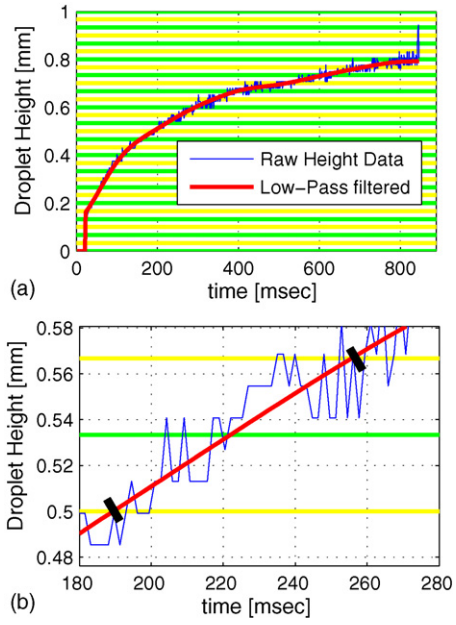

Fig. 6. (a, b) Example of raw and filtered droplet height signals (a) and magnification of the 0.500–0.566 mm bin (b).

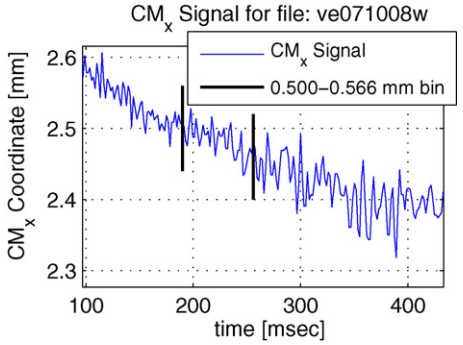

Fig. 7. Single segment of the horizontal center of mass signal.

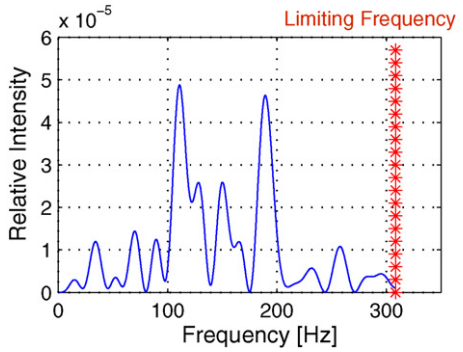

Fig. 8. Frequency spectrum for the 0.500–0.566 mm section of the horizontal center of mass signal above.

The limiting frequency on the right side of the plot represents the maximum frequency component which can be computed by the FFT, limited to half the sampling frequency. This spectrum shows two rough peaks, occurring around 110 and 190 Hz.

The primary aim of the frequency processing tools used was to identify the main oscillatory characteristics in droplets in the steady air stream. However, to be of any use, it was necessary to take many samples to check for consistency in the observed behavior in order to assure that the conclusions drawn are indicative of the actual physical reality. To this end, it was decided to perform the previously demonstrated experimentation and processing on a number of droplets observed at the same operating conditions. After performing a number of these, the frequency spectrum of all droplets at each size bin were algebraically averaged. The averaged spectrum is shown in Fig. 9. As this spectrum highlights, the higher of the two frequency peaks observed in Fig. 8 is maintained, while the lower point vanishes. This indicates that the higher frequency

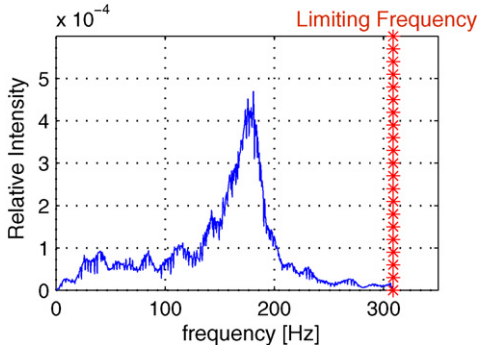

Fig. 9. Averaged frequency spectrum for the 0.500–0.566 mm section of the horizontal center of mass signal.

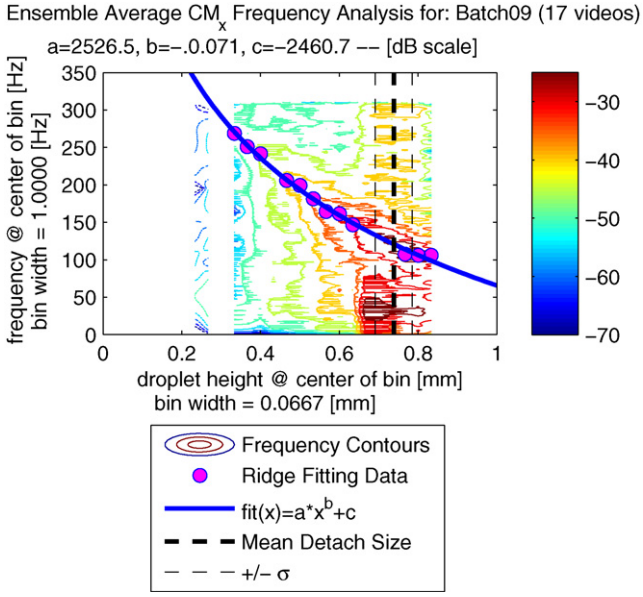

Fig. 10. Averaged frequency response over the entire droplet size range.

oscillation reflects actual behavior that is repeated in many droplets of this size.

As mentioned previously, the plots shown above have highlighted the process occurring for the 0.500–0.566 mm droplet size bin. These plots can effectively be thought of as slices out of the frequency-size plane, and the same process used to create the data plotted above was repeated over all the droplet size bins. Each data slice was then assembled, according to the droplet size it represents to create the plot seen in Fig. 10. After stacking the slices side-by-side, it becomes very clear that there exists a principle oscillatory trend over the range of droplet sizes monitored. This main ridgeline is alluded to by the contours plotted and is found more precisely by marking the peak frequency at which the highest oscillation amplitude occurs for each droplet size bin. This set of data points was used to generate a power series curve fitting which represents the primary oscillation frequency over the entire range of droplet sizes. As can be seen, this method of curve fitting agrees nicely with the ridgeline suggested by the contours.

In addition to monitoring the oscillatory characteristics of droplets, it is also helpful to record the critical size for each droplet in the batch. As shown in Fig. 11, the growth profiles for each droplet in the batch show strong similarity, as well as demonstrating a fairly tight collection of critical sizes. Statistics for the mean detachment size as well as the standard deviation in critical size were computed and plotted as well, and show strong similarity amongst droplets at similar conditions.

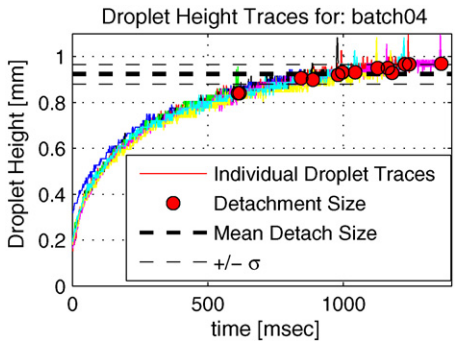

Fig. 11. Droplet height traces recorded for a single operating point batch with critical sizes marked.

Table 1
Summary of operating conditions examined.

Batch no.	No. of videos	Air flow rate (slpm)	Air velocity ($m\,s^{-1}$)	Air pressure (bar)	Water flow rate ($\mu l\,min^{-1}$)	Video frame rate (FPS)
4	13	140	14.5	1.08	0.8	510
12	22	140	14.5	1.54	0.8	490
5	8	170	17.6	1.52	1.0	510
7	20	190	19.6	1.76	0.8	510
9	17	210	21.7	2.02	0.8	616
10	17	228	23.6	2.28	0.8	616
11	26	245	25.3	2.48	0.8	616

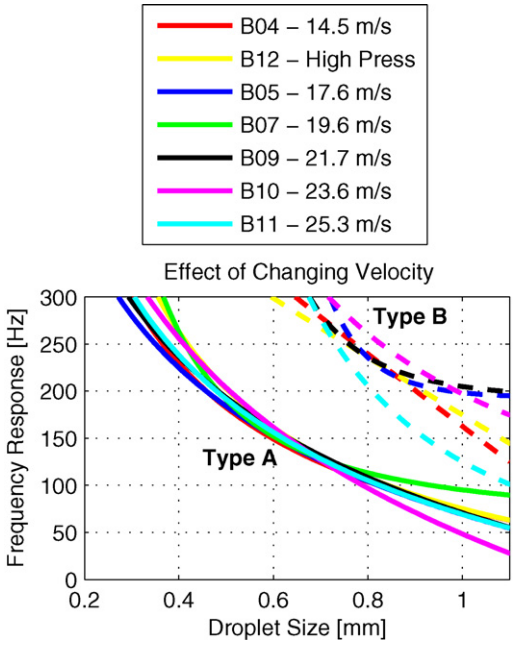

Fig. 12. Type A and B frequency trends.

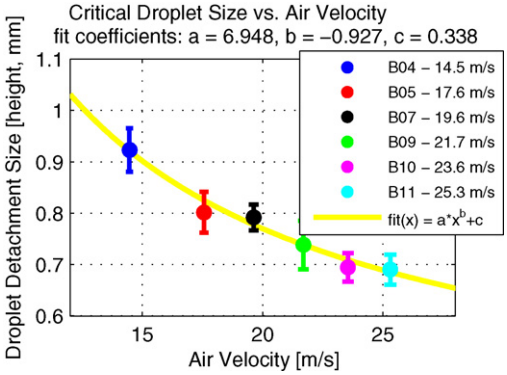

Fig. 13. Droplet critical sizes for range of flow velocities.

6. Results

The experimentation and data processing described above was conducted for several air flow conditions, as highlighted in Table 1, in an attempt to discern both the droplet oscillation dynamics as well as the critical detachment size characteristics at several points. The only two parameters changed throughout the course of the experiment were the air flow rate and pressure, with the temperature and humidity of the system at ambient.

While only the horizontal center of mass signal and spectra have been shown in the previous plots, as was stated earlier, a number of other signals have also been monitored. These signals can be divided into two groups according to the nature of the frequency trend they reflect. The first group, named Type A, is the group of signals including horizontal center of mass, droplet width, chord length and contact angles. The frequency behavior seen in these signals represents the horizontal mode of droplet deformation, which should be the strongest oscillation exhibited by the droplet as it is in the direction of air flow. The Type B frequency trend is exhibited by signals relating to vertical deformation, which are the droplet height and vertical center of mass.

These signals are expected to be weaker in amplitude than the Type A signals and are also expected to occur at higher frequencies due to a shorter vertical dimension of the droplet than the horizontal dimension.

The Type A and B trends for each of the operating conditions can be seen in Fig. 12. As the plot shows, there is strong agreement between the various Type A responses, while the Type B responses are grouped somewhat less tightly. The lower degree of closeness amongst the Type B curves is assumed to be a result of significantly less data for the estimation of these curves, since they are located near the corner of the size-frequency plane. The strong similarity found among the Type A curves indicates that flow conditions, either pressure or velocity, have no distinguishable effect on droplet oscillation frequencies.

This further indicates that the only parameter with a strong impact on droplet frequency behavior is droplet size, which seems to agree with simple mechanics reasoning as discussed in the next section. Therefore, all the Type A signals can be fit with a unique curve, which corresponds to the one illustrated in Fig. 10.

In addition to the oscillation trends, the detachment statistics have also been recorded and are plotted together in Fig. 13. Each batch data point shows a relatively small standard deviation, indicating fairly good repeatability between subsequent realizations. As the plot in Fig. 13 clearly shows, droplet size is inversely proportional to flow velocity, as expected. Furthermore, when the mean detachment sizes are fit with a power series curve, it is noted that the behavior from this somewhat limited set indicates a power law behavior.

7. Discussion

The oscillatory nature of the process involving the droplet attached onto the GDL surface and the air flow may be analyzed by analogy with the field of flow–structure interaction. To this purpose, the problem may be described by considering an elastic body immersed in a fluid flow. With this representation in mind, the oscillations are due to the elastic behavior of the droplet subject to the drag force. Therefore, in accord with the approach proposed by Blevins [24], the oscillating droplet can be represented as a mass-spring system. The natural oscillation frequency of such a system is $f_n = (1/2\pi)\sqrt{k/m}$, where f_n is the natural frequency, k is the spring constant and m is the mass.

To analyze the droplet oscillatory mechanism, an empirical relationship between oscillation frequency and droplet height was found as illustrated in Fig. 14.

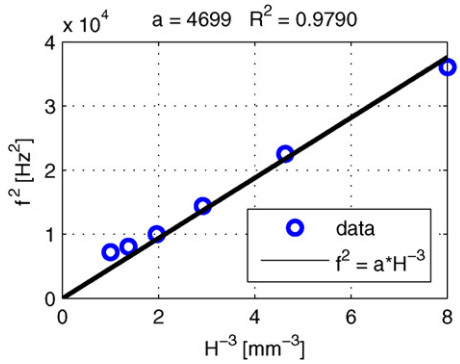

Fig. 14. Empirical correlation between droplet height and oscillation frequency.

As the curve fit shows, a linear trend can be assumed to describe the relationship between the inverse height cubed and the frequency squared. From this trend it may be argued that the droplet oscillation frequency is inversely proportional to the droplet volume and the aerodynamic force has no influence on the frequency. This result is in agreement with the above mentioned model presented by Blevins [24]. In analogy with the spring-mass system, it is fair to assume that the elastic behavior of the droplet is related to the surface tension. These considerations suggest the following law of proportionality:

$$f = \frac{1}{2\pi}\sqrt{\frac{G \cdot \sigma}{\rho \cdot V}} \tag{1}$$

where f and V are the droplet oscillation frequency and volume respectively, σ and ρ are the water surface tension and density respectively. G is a factor that accounts for the different geometry of the investigated system with respect to a mass-spring. In this work, G is assumed to be the curvature of the deforming droplet surface area:

$$G = \frac{\partial^2 S}{\partial x^2} \tag{2}$$

where S is droplet surface area and x is the longitudinal coordinate. Considering that the droplet deforms mainly along the longitudinal direction, a 2D section is taken and Eq. (2) can be written as:

$$G = \frac{\partial^2 S}{\partial x^2} = \alpha \frac{\partial^2 P}{\partial x^2} \tag{3}$$

where P is the perimeter of the 2D section and α is the ratio between droplet surface area and perimeter, i.e. it is $2r$ for a sphere of radius r. A quadratic curve is used to fit the droplet boundary perimeter in Fig. 5(b) and model its deformation. The droplet boundary perimeter equation is:

$$P(x) = 3.72 \cdot x_{CM}^2 - 1.37 \cdot x_{CM} + 1.18 \tag{4}$$

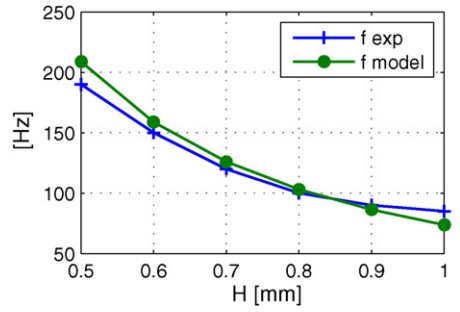

Fig. 15. Comparison between droplet experimental and estimated frequency.

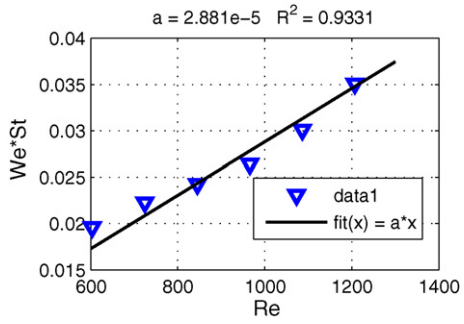

Fig. 16. Characterization of droplet oscillation through dimensionless groups: We*St vs. Re.

where x_{CM} is the center of mass x-coordinate in mm. Therefore, G is estimated as follows:

$$G = 2 \cdot r \cdot 7.42 = 2 \times 0.21 \times 7.42 = 3.12 \tag{5}$$

Fig. 15 shows that the droplet oscillation frequencies predicted by Eq. (1) and the experimental trend are in fairly good agreement.

A damping factor was not included in Eq. (1) since it impacts significantly on the oscillations amplitude, but it only slightly shifts the frequency. Obviously, a more accurate model should account for the mutual interaction between oscillating droplet and air stream. An aeroelastic model would be suitable to describe the nonlinear interaction and resonance phenomena [25]. However, such an approach is well beyond the objective of this work.

As concerns the droplet oscillation at detachment conditions, data analysis pointed out that the most representative dimensionless groups are the Reynolds number:

$$\mathrm{Re} = \frac{\rho_{air} \cdot v_{air} \cdot H}{\mu_{air}} \tag{6}$$

and a number accounting for the product $v_{air} \cdot H^2$, where v_{air} is the air velocity, ρ_{air} and μ_{air} are the air density and viscosity, respectively. Therefore, the other dimensionless group used to represent the detachment process accounting for the air flow induced vibration phenomena is:

$$We\,St = \frac{\rho H v_{air}^2}{\sigma}\frac{fH}{v_{air}} = \frac{\rho f v_{air} H^2}{\sigma} \tag{7}$$

It is important to notice that the characteristic length used in the dimensionless groups is the droplet height H. By processing the experimental data with Eq. (7), a linear trend with respect to Reynolds number was obtained as shown in Fig. 16.

Eq. (7) can be used to calculate the oscillation frequency of a droplet attached onto the GDL surface, given its size and the air velocity.

8. Conclusions

This work examined the nature of water droplet deformation and detachment characteristics in a simulated PEMFC flow channel. Using a fluorescence photometry imaging system along with a novel computational video processing routine, it was possible to estimate the principle horizontal and vertical deformation frequencies for droplets over a range of sizes. It was found that all the longitudinal signals (Type A) frequency trends fall into line with the same fitting power law. Moreover, it was noted that the droplet oscillation frequency does not depend upon air velocity, but is only influenced by droplet size. Furthermore, detachment characteristics were recorded, which indicate strong repeatability between droplet realizations. A plausible mechanisms of the droplet oscillation induced by the air flow was also provided along

with a dimensionless group analysis. These results may serve as an empirical basis for fuel cell water management studies for design, control and diagnostic applications.

Acknowledgments

The authors would like to thank the University of Salerno and the Center for Automotive Research at the Ohio State University for providing the opportunity for this collaborative work. Fruitful discussions with Mr Siefert and Prof Litster at the Carnegie Mellon University are kindly acknowledged. The authors are very grateful to Prof Luchini at the University of Salerno for his contribution on analyzing the droplet oscillation mechanism.

References

[1] H. Li, Y. Tang, Z. Wang, Z. Shi, S. Wu, D. Song, J. Zhang, K. Fatih, J. Zhang, H. Wang, Z. Liu, R. Abouatallah, A. Mazza, A review of water flooding issues in the proton exchange membrane fuel cell, J. Power Sources 178 (2008) 103–117.
[2] F. Barbir, H. Gorgun, X. Wang, Relationship between pressure drop and cell resistance as a diagnostic tool for PEM fuel cells, J. Power Sources 141 (2005) 96–101.
[3] W. He, G. Lin, T.V. Nguyen, Diagnostic tool to detect electrode flooding in proton-exchange-membrane fuel cells, AIChE J. 49 (2003) 3221–3228.
[4] M.M. Mench, Q.L. Dong, C.Y. Wang, In situ water distribution measurements in a polymer electrolyte fuel cell, J. Power Sources 124 (2003) 90–98.
[5] J.M.L. Canut, R.M. Abouatallah, D.A. Harrington, Detection of membrane drying, fuel cell flooding, and anode catalyst poisoning on PEMFC stacks by electrochemical impedance spectroscopy, J. Electrochem. Soc. 153 (2006) A857–A864.
[6] A. Esposito, C. Pianese, Y.G. Guezennec, A low order control-oriented model of liquid water transport in PEM fuel cell, 2008 ASME International Mechanical Engineering Congress and Exposition, October 31–November 6, Boston, USA.
[7] A. Turhan, K. Heller, J.S. Brenizer, M.M. Mench, Quantification of liquid water accumulation and distribution in a polymer electrolyte fuel cell using neutron imaging, J. Power Sources 160 (2006) 1195–1203.
[8] R. Satija, D.L. Jacobson, M. Arif, S.A. Werner, In situ neutron imaging techniques for evaluation of water management systems in operating PEM fuel cells, J. Power Sources 129 (2004) 238–245.
[9] M.A. Hickner, N.P. Siegel, K.S. Chen, D.S. Hussey, D.L. Jacobson, M. Arif, In-situ high resolution neutron radiography of cross-sectional liquid water profiles in PEM fuel cells, J. Electrochem. Soc. 155 (4) (2008) B427–B434.
[10] M.A. Hickner, N.P. Siegel, K.S. Chen, D.S. Hussey, D.L. Jacobson, M. Arif, Understanding the liquid water distribution and removal phenomena in an operating PEM fuel cell via neutron radiography, J. Electrochem. Soc. 155 (3) (2008) B294.
[11] K.R. Minard, V.V. Viswanathan, P.D. Majors, L.Q. Wang, P.C. Rieke, Magnetic resonance imaging (MRI) of PEM dehydration and gas manifold flooding during continuous fuel cell operation, J. Power Sources 161 (2006) 856–863.
[12] Z. Dunbar, R.I. Masel, Quantitative MRI study of water distribution during operation of a PEM fuel cell using Teflon flow fields, J. Power Sources 171 (2007) 678–687.
[13] T. Mukaide, S. Mogi, J. Yamamoto, A. Morita, S. Koji, K. Takada, K. Uesugi, K. Kajiwara, T. Noma, In situ observation of water distribution and behaviour in a polymer electrolyte fuel cell by synchrotron X-ray imaging, J. Synchrotron Radiat. 15 (2008) 329–334.
[14] I. Manke, C. Hartnig, M. Grünerbel, W. Lehnert, N. Kardjilov, A. Haibel, A. Hilger, J. Banhart, H. Riesemeier, Investigation of water evolution and transport in fuel cells with high resolution synchrotron X-ray radiography, Appl. Phys. Lett. 90 (2007) 174105.
[15] K. Tüber, D. Pócza, C. Hebling, Visualization of water buildup in the cathode of a transparent PEM fuel cell, J. Power Sources 124 (2003) 403–411.
[16] X.G. Yang, F.Y. Zhang, A.L. Lubawy, C.Y. Wang, Visualization of liquid water transport in a PEFC, Electrochem. Solid-State Lett. 7 (11) (2004) A408–A411.
[17] T. Ous, C. Arcoumanis, Visualization of water droplets during the operation of PEM fuel cells, J. Power Sources 173 (2007) 137–148.
[18] A. Bazylak, D. Sinton, N. Djilali, Dynamic water transport and droplet emergence in PEMFC gas diffusion layers, J. Power Sources 176 (2008) 240–246.
[19] S. Litster, D. Sinton, N. Djilali, Ex situ visualization of liquid water transport in PEM fuel cell gas diffusion layers, J. Power Sources 154 (2006) 95–105.
[20] E.C. Kumbur, K.V. Sharp, M.M. Mench, Liquid droplet behavior and instability in a polymer electrolyte fuel cell flow channel, J. Power Sources 161 (2006).
[21] A. Theodorakakos, T. Ous, M. Gavaises, J.M. Nouri, N. Nikolopoulos, H. Yanagihara, Dynamics of water droplets detached from porous surfaces of relevance to PEM fuel cells, J. Colloid Interface Sci. 300 (2006) 673–687.
[22] J.C. Berg, Wettability, Marcel Dekker, N.Y., 1993.
[23] A.D. Montello, An Experimental Investigation of Water Droplet Growth, Deformation Dynamics and Detachment in a Non-Reacting PEM Fuel Cell via Fluorescence Photometry, Thesis, 2008, OhioLINK ETD. http://www.ohiolink.edu/etd/view.cgi?acc_num=osu1228248650.
[24] R.D. Blevins, "Vortex–Structure Interaction, in Fluid Vortices" – Fluid Mechanics and its Applications, Kluwer Academic Press, 1995, pp. 533–574.
[25] A. Leonard, A. Roshko, Aspect of flow-induced vibration, J. Fluids Struct. 15 (2001) 415–425.